JGR Atmospheres

RESEARCH ARTICLE
10.1029/2019JD031770

Special Section:
Bridging Weather and Climate: Subseasonal-to-Seasonal (S2S) Prediction

Prediction of Northern Hemisphere Regional Sea Ice Extent and Snow Depth Using Stratospheric Ozone Information

Kane A. Stone[1], **Susan Solomon**[1], **and Douglas E. Kinnison**[2]

[1]Department of Earth, Atmospheric, and Planetary Science, Massachusetts Institute of Technology, Cambridge, MA, USA, [2]Atmospheric Chemistry Observations and Modeling Laboratory, National Center for Atmospheric Research, Boulder, CO, USA

Abstract The forecast potential of springtime ozone on April surface temperatures at particular locations in the Northern Hemisphere has been previously reported. Evidence suggests that early springtime Arctic stratospheric ozone acts as a proxy for extreme events in the winter polar vortex. Here, using a state-of-the-art chemistry-climate model, reanalysis and observations, we extend the forecast potential of ozone on surface temperatures to aspects of the Northern Hemisphere cryosphere. Sea ice fraction and sea ice extent differences between years of March high and low Arctic stratospheric ozone extremes show excellent agreement between an ensemble of chemistry-climate model simulations and observations, with differences occurring not just in April but extending through to the following winter season in some locations. Large snow depth differences are also obtained in regional locations in Russia and along the southeast coast of Alaska. These differences remain elevated until early summer, when snow cover diminishes. Using a conditional empirical model in a leave-three-out cross validation method, March total column ozone is able to accurately predict the sign of the observed sea ice extent and snow depth anomalies over 70% of the time during an ozone extreme year, especially in the region of the Bering strait and the Greenland Sea, which could be useful for shipping routes and for testing climate models.

Key Points:
- Excellent agreement between modeled and observed differences in Arctic sea ice extent and snow depth during March ozone extreme years
- Sea ice extent differences following March ozone extremes persist throughout the year in some locations
- Using ozone as the sole predictor, accurate forecasts of sea ice extent and snow depth anomalies are obtained during years of ozone extremes

Supporting Information:
- Supporting Information S1

Correspondence to:
K. A. Stone,
stonek@mit.edu

Citation:
Stone, K. A., Solomon, S., & Kinnison, D. E. (2020). Prediction of Northern Hemisphere regional sea ice extent and snow depth using stratospheric ozone information. *Journal of Geophysical Research: Atmospheres*, *125*, e2019JD031770. https://doi.org/10.1029/2019JD031770

Received 2 OCT 2019
Accepted 22 OCT 2020
Accepted article online 29 OCT 2020

1. Introduction

The connection between the Arctic stratosphere and surface weather and climate has been an area of growing scientific interest in recent years (Scaife et al., 2016; Sigmond et al., 2013). Stratospheric ozone is measured routinely to extremely high accuracy and precision. Therefore, its close relationship to the state of the Arctic polar stratosphere, especially in the winter months, makes it a useful resource to investigate the impact of stratospheric anomalies on different surface variables. The cryosphere is of particular interest in this paper.

It has been previously shown that there is a strong connection between springtime polar stratospheric ozone and regional surface temperatures in subsequent months in both hemispheres. In the Southern Hemisphere this connection is seen most prominently in South East Australia in observations (Bandoro et al., 2014). However, in models, similar strength connections in Australia are most prevalent in simulations with prescribed observed sea surface temperatures (Gillett et al., 2019). In the Northern Hemisphere, March Arctic stratospheric ozone extremes show strong correlations with Northern Hemisphere regional surface temperatures in April in both observations (Ivy et al., 2017) and models (Calvo et al., 2015; Stone et al., 2019), most noticeably across Russia and Southern Asia. Additionally, there is excellent agreement between the observations and an ensemble of Whole Atmosphere Community Climate Model (WACCM) simulations, which allowed the tropospheric climate link to ozone to be used to predict the sign of regional surface temperature anomalies in parts of Russia and Southern Asia accurately during ozone extremes (Stone et al., 2019).

Understanding the role of Arctic stratosphere-troposphere coupling on regional surface climate has been a focus of several studies. For example, Baldwin and Dunkerton (2001) showed that large Arctic stratospheric circulation anomalies in the winter have an effect on the surface over the following months. Additionally, Charlton-Perez et al. (2018) showed that a negative phase of the Northern Annular Mode (NAM) is most sensitive to a weak winter Arctic stratospheric vortex, and vice versa for a positive NAM, and the stratosphere's predictability for extratropical surface temperatures arises from prediction of the NAM (Jia et al., 2017).

Further, the response of Arctic sea ice to anomalous NAM has been documented extensively, with wintertime NAM having a strong influence of Arctic sea ice through the spring and summer (Kwok, 2000; Rigor et al., 2002; Stroeve et al., 2011; Wettstein & Deser, 2014; Williams et al., 2016). One mechanism of stratospheric-troposphere coupling has been attributed to planetary wave-reflection in the stratosphere (Perlwitz & Harnik, 2003), with abnormal tropospheric wave-activity originating from sea ice and snow cover anomalies and mediated by the stratosphere, for example, in the Barents-Kara sea (Zhang et al., 2018). However, other proposed mechanisms include redistribution of potential vorticity control (Hartley et al., 1998), and wave-mean flow interactions (Baldwin & Dunkerton, 2001; Plumb & Semeniuk, 2003; Polvani & Waugh, 2004), among others (see Garfinkel et al., 2013).

Unlike the Southern Hemisphere, where it is well established that anthropogenic springtime ozone depletion causes a strong modulation of the stratospheric polar vortex, and in turn, surface weather in the austral summer (e.g., Thompson et al., 2011), the causal role of Arctic ozone changes on stratospheric circulation anomalies and subsequent tropospheric changes in the Northern Hemisphere is less well established. Considering that large Arctic anthropogenic ozone depletion only occurs intermittently, ozone variability is likely mostly dynamically driven. However, as long as chlorine concentrations remain high, the variability is likely enhanced through ozone loss feedbacks. Indeed, there is some evidence that there are positive ozone feedback effects during years of Arctic stratospheric temperature and circulation anomalies (Haase & Matthes, 2019; Romanowsky et al., 2019). Additionally, years of large NH anthropogenic ozone depletion, such as 2011, have been shown to coincide with large regional tropospheric temperature anomalies (Stone et al., 2019). This agrees with a previous study that suggested the ozone anomalies contributed to the predictability of European spring climate in 2011 (Karpechko et al., 2014), however, another study found no causal link (Cheung et al., 2014). Arctic stratospheric ozone has also been linked to changes in tropical rainfall at very long lead times (Xie et al., 2017), and precipitation in North America (Ma et al., 2019). Harari et al. (2019) suggested that an ensemble of chemistry-climate models displays ozone correlations with tropospheric climate that stem from correlation with El Niño–Southern Oscillation (ENSO) rather than a causal effect. The focus of this paper is on the usefulness of stratospheric ozone for prediction of Northern Hemisphere sea ice and snow depth, which does not depend on whether any connections are causal or not. Using ozone, and total column ozone (TCO) especially, has the additional benefit of being measured very accurately over a long period of time, and accurate values are routinely available in near real-time, adding to its usefulness for prediction.

Considering the strong link between the wintertime stratosphere, and hence stratospheric ozone, on regional surface temperatures, the question arises whether the same link is captured in the Northern Hemisphere cryosphere. Indeed, Smith et al. (2018), found strong connections between Arctic stratospheric winter circulation anomalies and sea ice in the Barents-Kara Sea over the following months. Additionally, Kelleher et al. (2020) found connections between the timing of the stratospheric final warming and Arctic sea ice. Here, we investigate whether these anomalies are also captured in an ozone proxy, and extended over other aspects of the entire cryosphere domain, such as snow depth. Further, we examine the effectiveness of the ozone proxy for prediction of surface cryosphere anomalies throughout the remainder of the year.

2. Data

The model and observational data used in this study are similar to that used in Stone et al. (2019), with the exception of MERRA2 data used for sea ice fraction and snow depth instead of ERA-Interim (a description of which is below). The model used is the WACCM version 4 (WACCM4) module of the Community Earth System Model, version 1 (CESM1). This is a fully coupled chemistry climate model that has a horizontal resolution of 1.9° latitude by 2.5° longitude and up to 66 vertical levels with a high top at 5.1×10^{-6} hPa (~140 km) (Garcia et al., 2017; Marsh et al., 2013). Total column ozone (TCO) observations are from the National Institute for Water and Atmosphere-Bodeker Scientific total column ozone database V3.2 patched data set (Struthers et al., 2009). Nine ensembles based on the REF-C2 forcings from Phase-1 of the Chemistry Climate Model Initiative are used (Morgenstern et al., 2017), over the time period of 1995–2024. See Stone et al. (2019) or the supporting information for more in depth details.

The Modern-Era Retrospective Analysis for Research and Applications, Version 2 (MERRA2), produced by NASA's Global Modeling and Assimilation Office are used for the "observed" sea ice fraction, snow depth,

and zonal wind data (Gelaro et al., 2017). Observations in conjunction with a forecast model are used to create the data set, which spans the period of 1980 to present. We use monthly mean MERRA2 sea ice fraction and total land snow storage data with a resolution of 1.5° latitude by 1.5° longitude over the period of 1980–2016. We also use daily MERRA2 10 hPa 60°N zonal wind. We find that the results for sea ice fraction in MERRA2 and ERA-Interim are very similar. However, snow depth in ERA-interim is not consistent with other reanalysis products (e.g., Broxton et al., 2016). Therefore, MERRA2 is used in this study. Comparison of MERRA2 sea ice fraction with observational data sets from the National Snow and Ice Data Center show very similar results. Therefore, MERRA2 was used in this study. See Figure S8.

When discussing both the observed TCO and MERRA2 data together, we refer to them as observations.

3. Methods

The methodology used in this paper for sections 4.2–4.5, including the calculations of significance, is similar to that based on our study of the predictability of Northern hemisphere surface temperature connections to ozone. An abbreviated version is shown here. Refer to Stone et al. (2019) or the supporting information for further details.

Sea ice fraction, sea ice extent, and snow depth differences shown in sections 4.2 and 4.3 were calculated by first preconditioning the data sets by removing the linear trends from TCO, and removing the linear trends and ENSO (defined as the NINO 3.4 index) from the sea ice fraction and snow depth data. This was performed by removing the linear least squares regression fits of the linear and ENSO regression functions from the data sets. The modeled composites of sea ice fraction and snow depth differences were then constructed from the data points that correspond to the March 63–90°N TCO extreme values (upper 20th percentiles minus the lower 20th percentiles) for each model ensemble member individually and observations. Sea ice extent is calculated by assuming sea ice is present when the sea ice fraction is greater than 0.15 in each grid cell separately. The area-weighted sea ice extent is then calculated by summing the areas of all grid cells that meet this criterion. Significance is based on a two-tailed student t test at the 95th percentile.

Regression analysis shown in section 4.4 uses a linear least squares regression model with mean March 63–90°N TCO as the sole predictor of the sea ice extent and snow depth predictands for the following months in the year. The regression model training periods are 1980–2010 for observations, and 1995–2020 for the model, with the remaining 6 and 4 years predicted for observations and the model respectively. Preconditioning of the data sets involved removing the linear and ENSO influence through their linear least square regression fits. However, only data from the training periods were used to remove the linear trend and ENSO. This ensures that no forecasted data are used in construction of the model.

A conditional empirical model is used to predict the sign of the sea ice extent and snow depth anomalies through the construction of leave-three-years-out Heidke skill scores (HSSs) in section 4.5. This methodology is similar to Stone et al. (2019) and based on the sign of the surface variable difference from the March TCO upper 20th percentiles minus the March TCO lower 20th percentiles. For the nine model ensemble members, 30 consecutive empirical models are produced after each three consecutive data points are left out. The remaining 27 data points are the training data sets. Each separate empirical model is then used to predict the middle point that was left out. For the 9-member ensemble this results in 270 forecasts of which the HSSs are calculated by

$$HSS = \frac{H - E}{T - E} \times 100 \tag{1}$$

where H is the number of correct predictions, T is the number of forecasts (in this case, 270), and E is the number of correct forecasts by chance ($T/2$ in this case). The HSS values range from −100 to 100, with 0 being an equal number of correct and incorrect forecasts. A positive value means more correct forecasts than incorrect forecasts and vice versa. See Stone et al. (2019) and section S1 for more details. Significance of the HSSs are constructed after the model predictions are bootstrapped 2,000 times, the HSSs are recalculated, and the 95th percentile of the bootstrapped samples is determined. This gives an indication of the HSS variability by chance given the sample sizes used, and therefore confidence in the predictions that lie outside of this range.

4. Results

4.1. Arctic Winter Polar Vortex and TCO

Figure 1 shows how daily March Arctic TCO and zonal wind at 10 hPa and 60°N (a standard metric for the strength of the polar vortex) are related to each other over the course of the winter for both observations and the model ensemble. This is highlighted by plotting the upper and lower 20th percentiles of the 63–90°N averaged March TCO (panels a and b) together with the corresponding zonal wind time series over the entire year (panels c and d). As expected, the largest differences between the ozone extreme years occur in March (as March was used to construct the extremes), but the separation between the mean values of the two extreme sets of data begins at the start of November in both the model and observations. This behavior is reflected in the zonal wind metric, with differences also becoming evident at the start of November (Figures 1c and 1d). In both the observations and the model, during upper ozone extreme years, there are a large number of sudden stratospheric warmings (where the wind direction becomes easterly), and conversely, during the lower ozone extremes, there are a larger number of strong polar vortex (SPV) events, defined here as cases when the wind speed goes above 40 m s^{-1} as this is the value that gives a similar amount of SPVs compared to SSWs. However, the observations show much stronger SPV events compared to the model, with wind speeds exceeding that of the entire model ensemble. In the observations, three of the March upper ozone extreme years that had a SSW were succeeded by a SPV event, and were then typically followed by a later SSW or an early final warming. This is also seen in the model (not explicitly shown here), with the majority of SPVs that occurred during upper ozone extreme years being followed by a SSW or an early final warming. Whereas, lower extreme ozone years are characterized by both SPVs and a more stable vortex over the entire winter. Indeed, the variability of the zonal wind is much larger during the years that correspond to March upper ozone extreme years compared to lower ozone extreme years in both the observations and the model (see Figure S1). This indicates that March ozone extremes are influenced by both the state of the vortex over the entire winter and by extreme polar vortex events. This gives confidence that we cannot only use ozone as a proxy for SSW and SPV events but also for the strength of the polar vortex throughout the winter.

4.2. Sea Ice Fraction and Extent Differences During Ozone Extremes

Figure 2 shows the seasonal change in sea ice fraction due to the difference between the March ozone extreme years (upper TCO 20th percentile years minus the lower TCO 20th percentiles years) for both observations and the model ensemble mean. For the April, May, and June season (panels a and d), there are large positive sea ice fraction differences outside of the Arctic Ocean in the Bering Sea and the Sea of Okhotsk in both observations and the model ensemble. There is also agreement in the Barents Sea region, with both observations and the model showing positive anomalies. These differences extend into the Kara Sea region in both the model and the observations, but with a larger difference in the observations. In the Greenland Sea, Hudson Bay, and Baffin Bay, negative anomalies are obtained, with a magnitude that is larger in the observations than the model. Overall, there is excellent agreement in the regional structure of the sea ice fraction differences between the model and observations, and agrees well with Smith et al. (2018). These results also agree well with Kelleher et al. (2020), further indicating that SSWs, SPVs, and the stability of the vortex all play a part in how wintertime ozone acts as a proxy for the polar vortex's influence on the troposphere.

During the late summer and early autumn periods (panels b and e), sea ice has retreated entirely into the Arctic Ocean, and large positive sea ice fraction differences are seen in the Laptev, East Siberian, Chukchi, and Beaufort Seas in the model, and in the Laptev, Chuchki, and the southern part of the Beaufort Seas in the observations. However, the positive differences in the observations are not as significant as the model and are flanked by negative anomalies further north. The Greenland Sea shows large negative anomalies during this time period, especially along the North East Greenland region and near Svalbard. We note that the difference in sea ice fraction during ozone extreme years that do not correspond to a wintertime SSW or SPV events is very similar (see Figures S2–S4). This indicates that ozone extremes are also capturing smaller stratospheric winter anomalies in the absence of SSWs or SPVs.

As sea ice begins to expand again during the late autumn and early winter period (panels c and f), there are still large sea ice fraction differences in the Bering Strait in both the model and observations, showing

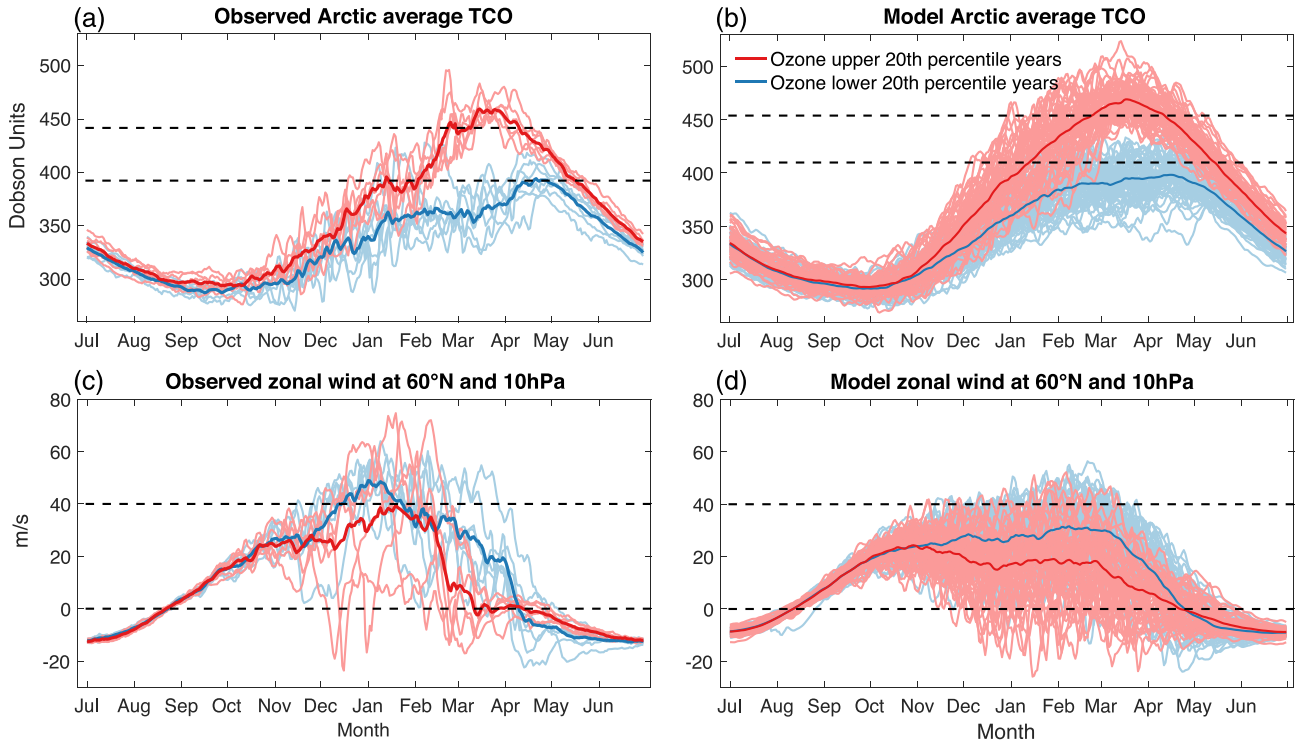

Figure 1. Coincident time series of daily 63–90°N average March total column ozone and zonal wind at 60°N and 10 hPa during March total column ozone extreme 20% highest (red) and lowest (blue) years for observations (a and c) and across all ensemble members (b and d). Black dashed lines indicate the ozone ensemble composite upper and lower 20th percentile values (panels a and b), and SSW and SPV limits (panels c and d).

substantial persistence in sea ice fraction changes in this region. There are also still small differences along North East Greenland. However, the large observed differences in the Kara Sea and Baffin Bay are not seen in the model.

Figure 3 shows the monthly sea ice extent differences within the regions shown in Figure 2. Again, we see good agreement between observations and the model ensemble. In the Barents-Kara sea (panel a), we see the largest positive differences occurring around May, June, and July in both the observations and the model. However, there is large variation among ensemble members shown as the standard deviation among the different members. Later in the year, the sign of the observed difference changes, with negative anomalies seen in October and November. This is only slightly captured in the model composite, where the difference only reduces to zero in September.

Panel (b) shows the monthly sea ice extent difference for the region that covers the Pacific areas of the Sea of Okhotsk and the Bering Sea, and the Arctic Seas of the Laptev, East Siberian, Chukchi, and Beaufort Seas (OBCLEB). After June, the sea ice is confined to the Arctic Ocean. In the earlier part of the year (up to May) the sea ice extent differences are solely arising from the Pacific seas, and later in the year, the differences are arising from the Laptev, Eastern Siberian, Chukchi, and Beaufort Seas. Again, excellent agreement is obtained between the model and the observations, with the largest sea ice extent differences occurring in May of 4×10^5 km^2 before the sea ice retreats to within the Arctic Ocean. However, after May, positive sea ice extent differences are still seen within this region in the Arctic Ocean, with consistency throughout the rest of the year and differences ranging from 0 to 2×10^5 km^2.

Differences in the Barents-Kara Sea region have been shown to be associated with sea ice advection rather than changes in sea ice thickness. Whereas, differences in the OBCLEB region are associated with changes in sea ice thickness (see Smith et al., 2018, and references therein).

In the Greenland Sea (panel c), the differences in sea ice extent are negative throughout the entire year but become more pronounced after April in both the observations and the model. In the observations the

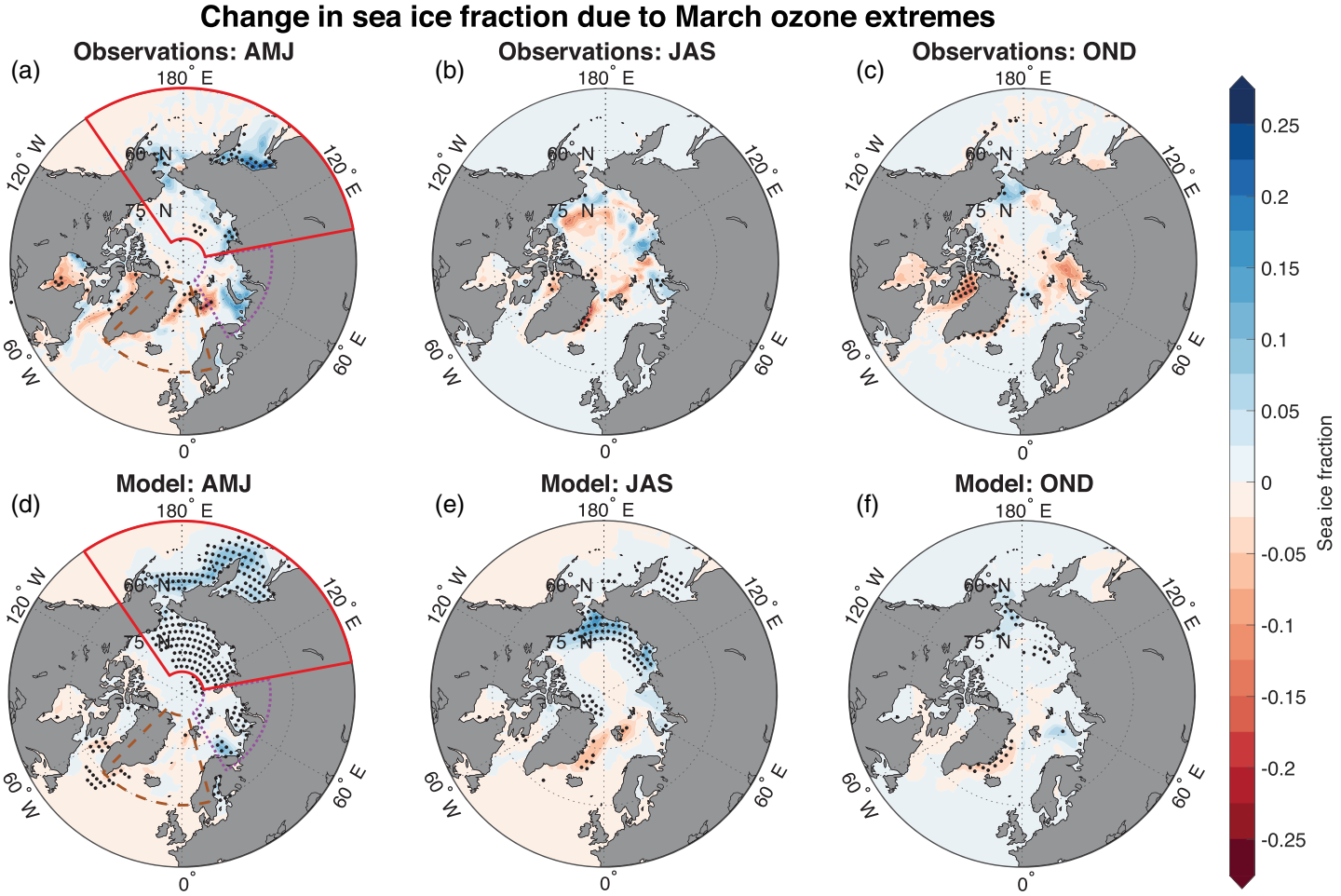

Figure 2. (a–f) MERRA2 and WACCM ensemble sea ice fraction differences corresponding to years of March ozone extremes (upper 20th percentile minus lower 20th percentile). Boxes correspond to sea ice extent differences shown in Figure 3. Hatched areas show significance at the 95% confidence interval. Boxed areas show the regions used for Figure 3. The red solid box is Sea of Okhotsk and the Bering Sea, and the Arctic Seas of the Laptev, East Siberian, Chukchi, and Beaufort Seas (OBCLEB). The purple dotted box is the Barents-Kara Sea. The brown dashed box is the Greenland Sea.

differences peak in July at around -1.5×10^5 km^2 before reducing to -0.5×10^5 km^2 in October through December. In the model, the differences peak in September at approximately -1.0×10^5 km^2 before similarly reducing to -0.5×10^5 km^2 from October through December. However, the only months in the model composite differences that are outside of the ensemble standard deviation are August and September. The lower sea ice fraction values within the Greenland Sea agree with previous studies on advection of sea ice out of the Arctic through the Fram Strait associated with a positive phase of the NAM (e.g., Kwok, 2000; Rigor et al., 2002). Regression of the NAM on sea ice fraction anomalies in the model shows a similar pattern to the TCO composite anomalies, with a negative NAM associated with positive TCO composite sea ice fraction anomalies (see Figure S5). This indicates that the surface response to the TCO proxy is largely through modulation of the NAM and is in agreement with Jia et al., 2017.

The OBCLEB region is much larger than the other two regions shown here, and this may contribute to the lower variability within that region compared to the other two. However, sea ice fraction difference in the OBCLEB region is also remarkably consistent among ensemble members during April-May-June. There are more visible inconsistencies between ensemble members for the other regions over April-May-June and July-August-September. See Figures S6 and S7.

Overall, it is clear that in both observations and the model, there are large sea ice fraction and sea ice extent differences that correspond to March ozone extreme years. The magnitude of the changes between the

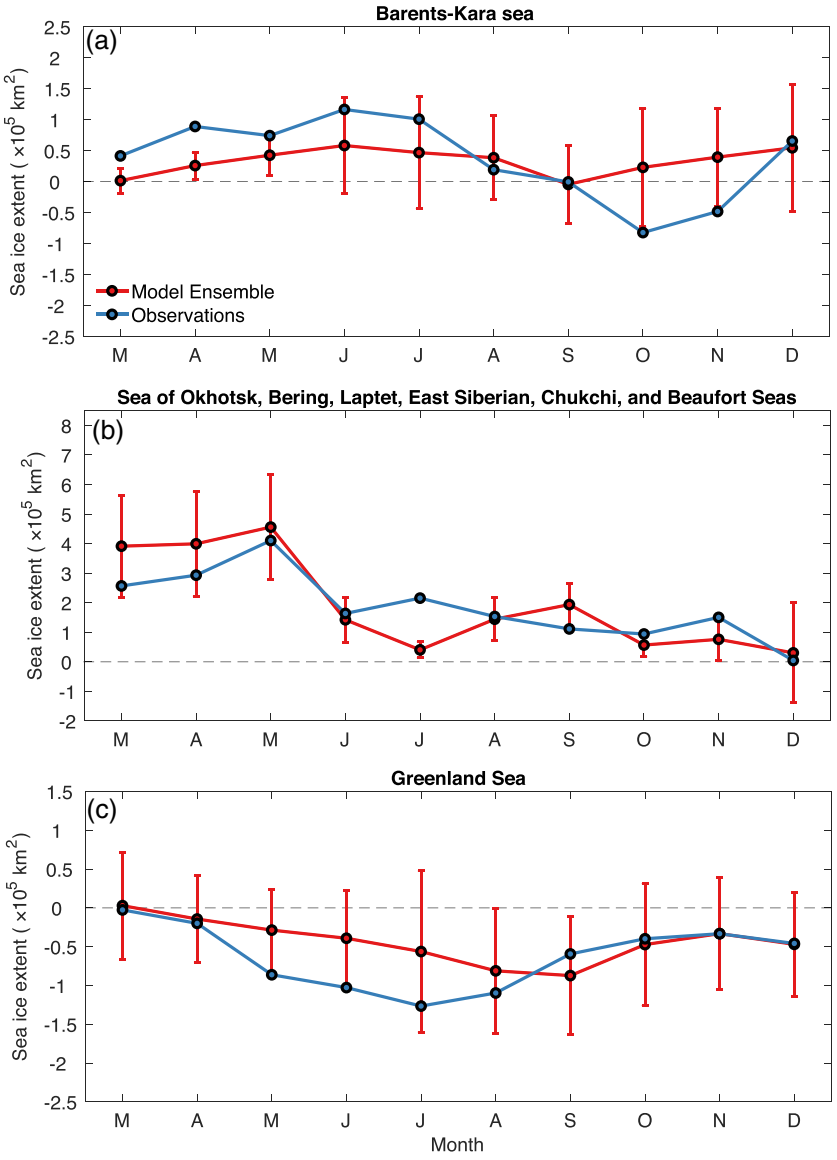

Figure 3. MERRA2 and WACCM subsequent sea ice extent differences corresponding to years of March ozone extremes for the locations shown in Figure 2. The error bars are the model ensemble one standard deviation.

model and observations are very similar during all months across the three locations. However, there is a large amount of variability among the ensemble members in the Barents-Kara and Greenland Seas. In the Laptev, Eastern Siberian, Chukchi, and Beaufort Seas, and within the Bering Strait, the differences are much more consistent among ensemble members and observations and persistent throughout the remainder of the year. This persistence has implications for shipping routes into the Arctic, especially through the Bering Strait, where the model shows the most consistency among members. These results are consistent with Smith et al. (2018).

4.3. Snow Depth Differences During Ozone Extremes

In this section the influence of the Arctic winter polar vortex on regional snow depth within the Northern Hemisphere is explored, in a manner similar to the previous section.

Figure 4 shows the snow depth changes during March ozone extreme years. Both the observations and the model capture positive snow depth anomalies in the Southern Russia and South East Alaskan regions, and

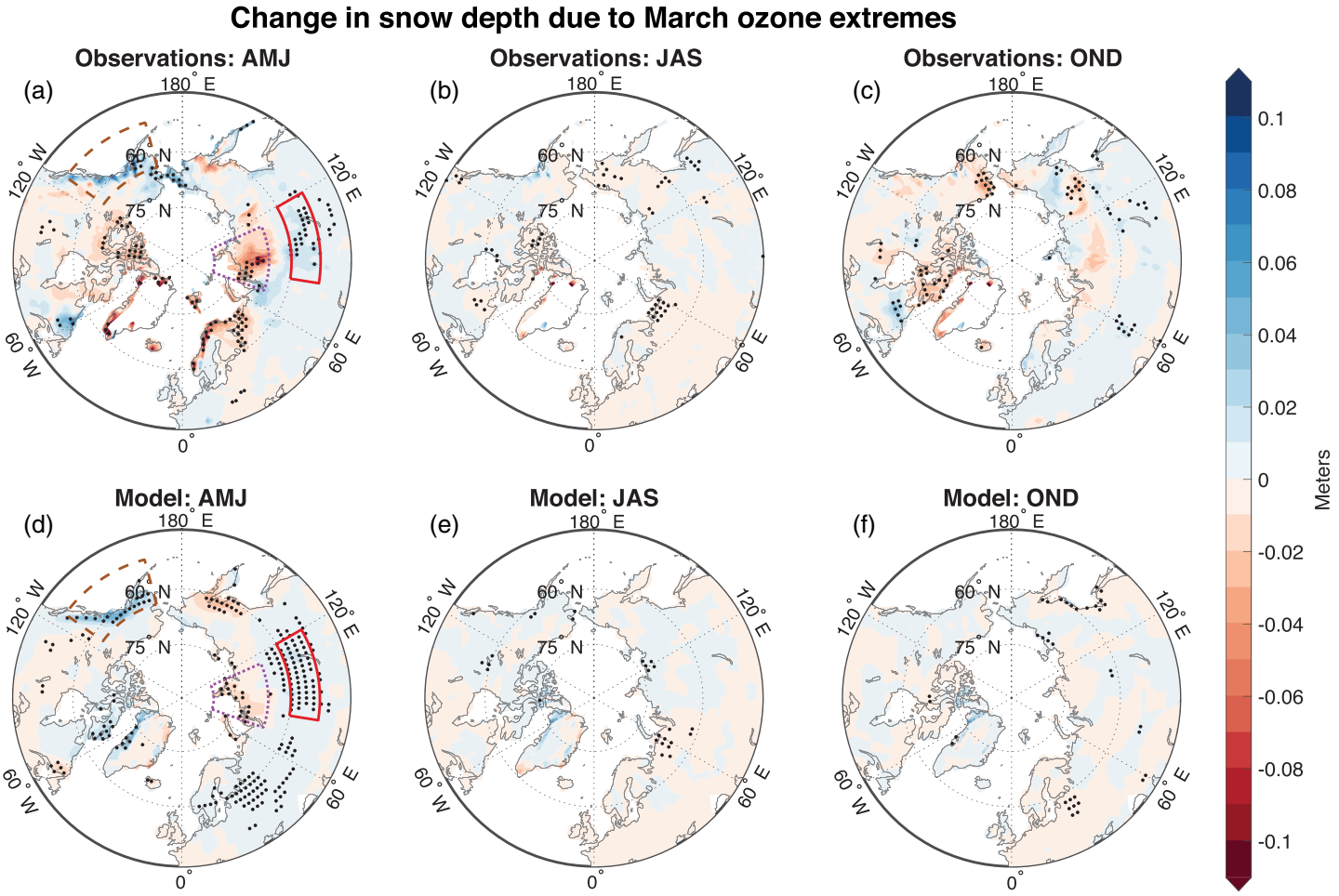

Figure 4. (a–f) MERRA2 and WACCM ensemble snow depth differences corresponding to years of March ozone extremes (upper 20th percentile minus lower 20th percentile). Boxes correspond to snow depth differences shown in Figure 5. Hatched areas show significance at the 95% confidence interval. Boxed regions show the areas used for Figure 5. The red solid box is the Northern Russian region. The dashed brown box is the South East Alaska region.

negative snow depth differences are in the Northern Russian region, with good agreement between the model and observations. However, there are also some differences between the model and the observations in other regions, with large negative differences seen in the observations along the Northern Scandinavian region which is not captured in the model.

The Northern Russia region of large snow depth differences is in a similar location of very large negative surface temperature differences (Stone et al., 2019). Additionally, the large modeled differences in snow depth coincide very strongly with large differences in snow precipitation (see Figure S9). Even though all these changes are linked to modulation of the NAM (see Figure S5 for sea ice response to NAM), for example, similar precipitation changes along South East Alaska were discussed in Ma et al. (2019) and linked to stratospheric modulation of the NAM, the exact drivers require further investigation and is not the purpose of the this paper.

Figure 5 shows the snow depth differences within the three regions highlighted in Figure 4. In Northern Russia, the negative snow depth differences peak in April in both the observations and the model but remain elevated through to June. However, the observations show a much larger difference. In Southern Russia, there is good agreement between the model and the observations, with positive snow depth differences peaking in April before reducing to zero in June. The differences in South Eastern Alaska peak strongly in May in the observations, while the model shows the largest differences from March through to May. The observations also remain elevated through to August as opposed to July and June in the other regions.

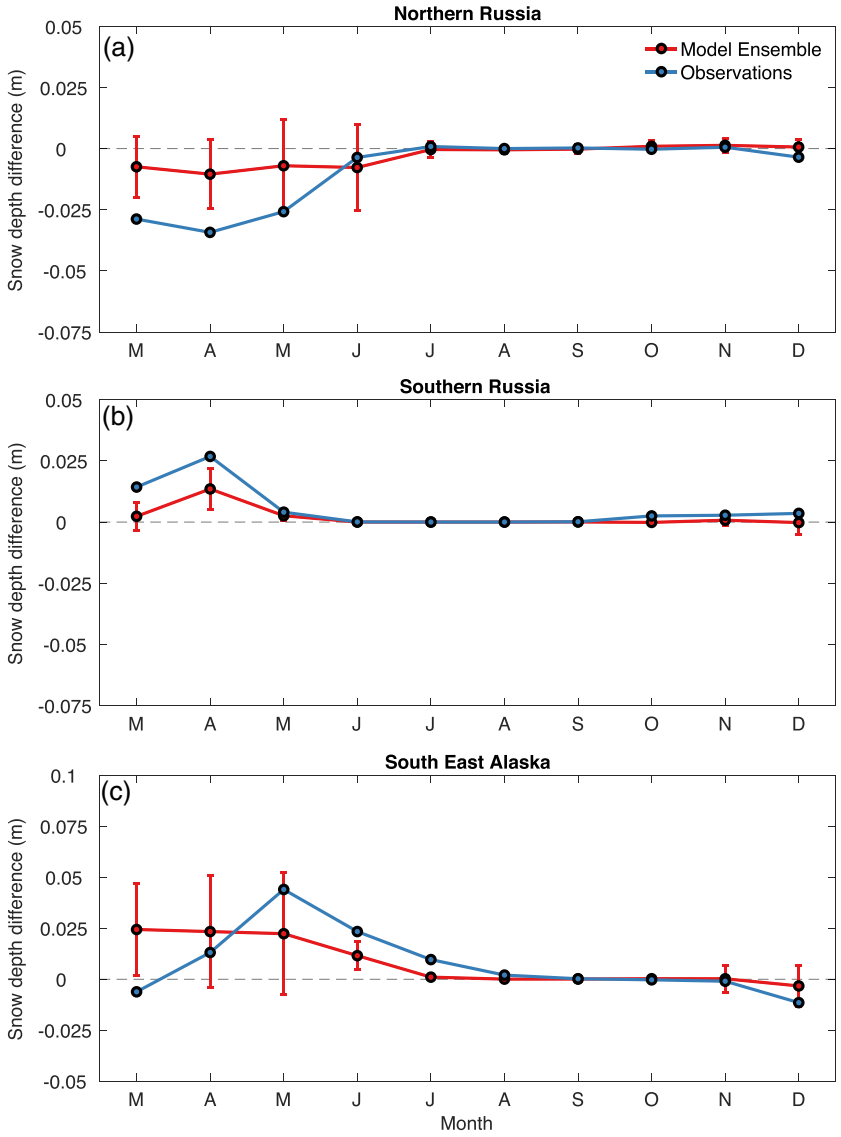

Figure 5. (a–c) MERRA2 and WACCM average snow depth differences corresponding to years of March ozone extremes for the locations shown in Figure 4. The error bars are the ensemble one standard deviation.

Also, contrary to sea ice fraction differences, snow depth differences are confined almost entirely to the spring and early summer periods, since snow entirely disappears later in the year.

4.4. Prediction Through Simple Linear Regression

Using a linear regression model described in section 3, here we use March ozone as the sole predictor to predict future sea ice extent and snow depth in selected locations shown in Figures 2 and 4. The predictions are made over 6 and 4 consecutive years in observations and the model, respectively. This is designed to investigate predictive variability among ensemble members and if the relationship between March ozone and sea ice extent and snow depth holds over an extended period of time.

For sea ice extent, the region that encompasses OBCLEB is chosen with predictions made for May considering this month showed the largest difference in sea ice extent between years of upper and lower ozone extremes. For observations in this region (Figure 6a), the regression model over the period of 1980–2010 does a reasonable job of replicating the observations, with a correlation between ozone and sea ice extent of 0.48. Using the model, predictions are made for the remaining 6 years of 2011–2016. During 2011, which is a year

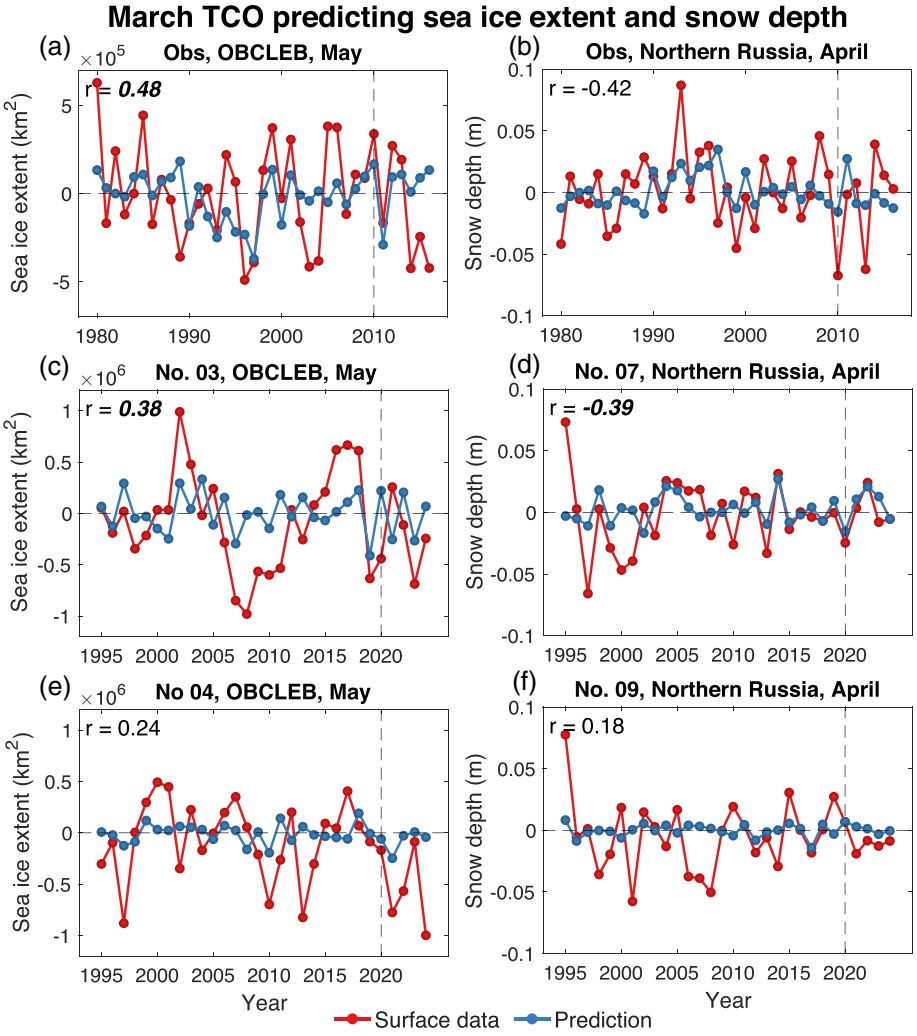

Figure 6. Observed march 63–90°N TCO and 1980–2010 regression model fits and 2011–2016 predictions of MERRA2 and model May sea ice extent for OBCLEB, and April snow depth for Northern Russia (a and b). Similarly, for ensemble members 3 and 4 (c and e) for sea ice extent in OBCLEB, and ensemble members 7 and 9 (d and f) for snow depth in Northern Russia. A model regression model time period of 1995–2020 was chosen with forecasts over 2021–2024. *r* is the Pearson correlation coefficient taken over the training period. *r* values that are bold italics are significant to the 95th percentile.

of large Arctic ozone depletion, we see good prediction, with a similarly large deviation in the actual sea ice extent data. The predictions also do a reasonable job for 2012 and 2013 but do not capture the large negative sea ice extent anomalies for the following years. Examples of two individual ensemble members for this same region are shown in Figures 6c and 6e. The two examples chosen highlight the variability among the ensemble members. For ensemble member 3, we see reasonable predictions for three out of the 4 years, while ensemble member 4 has poorer predictions for this region. Further ensemble members are shown in Figure S10 for different regions.

Figure 6b shows similar predictions for snow depth in the Northern Siberia region. The regression model has a reasonable fit with a correlation of March ozone and snow depth of −0.42; however, the correlation is not significant to the 95th percentile. The predictions for 2011–2016 track the snow depth data reasonably well, however, the magnitudes are quite different. Two model ensemble members are shown in Figures 6d and 6f. In this region, the variability between ensemble members is much greater, as seen with ensemble members 7 and 9 which show a different correlation sign. However, for the members that do show a reasonable regression model fit (Figure 6d), the predictions over the 2021–2024 are good. Considering that there is clear

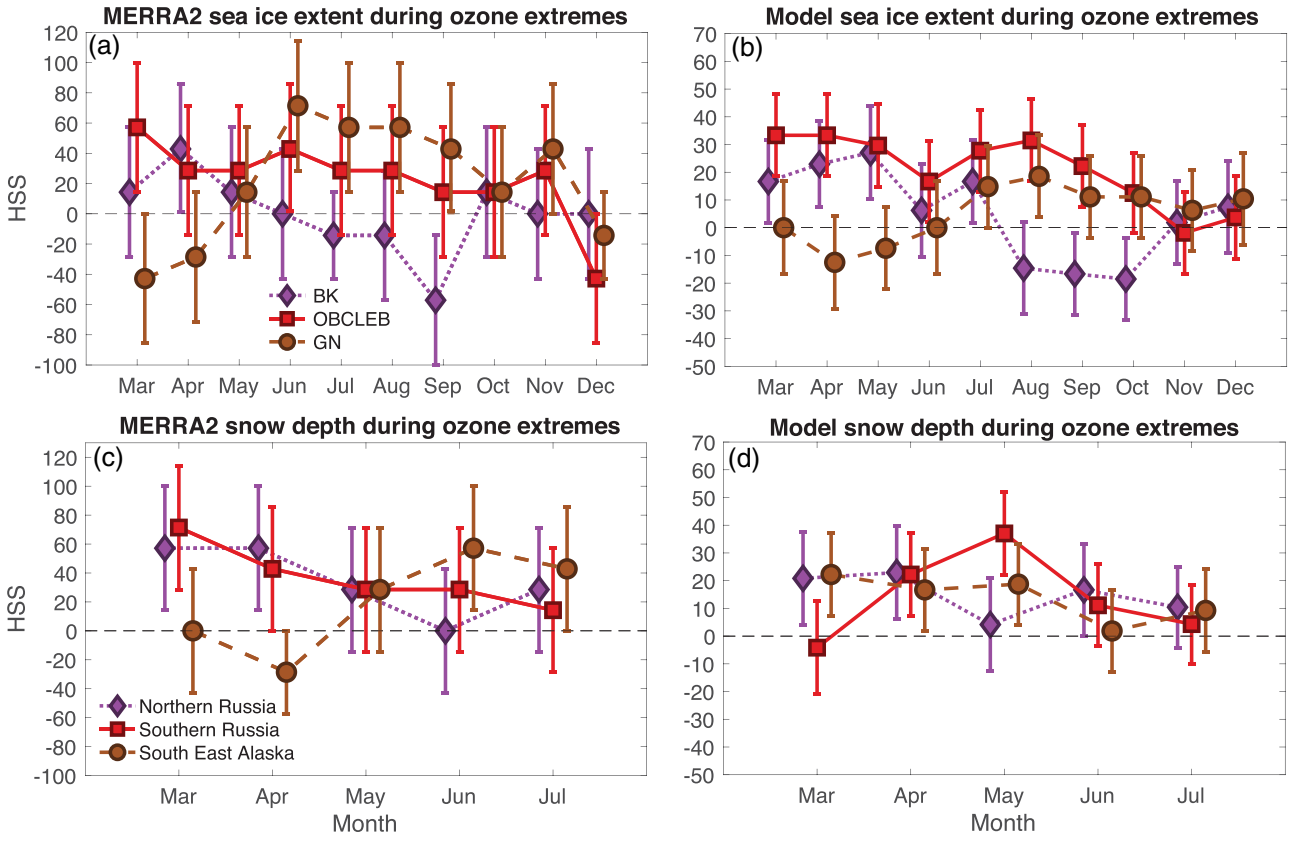

Figure 7. Observed and modeled HSSs for sea ice extent in the locations shown in Figure 2a (a and b). This is shown for years that correspond to March ozone extremes. Similarly, snow depth in the locations shown in Figure 4a is presented in panels c and d. Note the different y axis limits between observations and the model ensemble mean. For sea ice extent, the different regions are BK: Barent-Kara Sea; OBCLEB: Sea of Okhotsk, Bering, Laptev, Chukchi, East Siberian, and Beaufort Seas; GS: Greenland Sea. Significance is shown at the 95th percentile of 2,000 bootstrapped samples.

variability in the correlations and prediction of the cryosphere among different ensemble members, a more appropriate approach is to focus on predicting the sign of the anomalies during ozone extreme years (during which large stratospheric anomalies occur), presented in the next section.

4.5. Leave-Three-out Anomaly Prediction

Following the large sea ice extent and snow depth differences that are occurring during years of ozone extremes in both observations and the model ensemble, the question arises as to whether the sign of the sea ice extent and snow depth anomalies can be predicted using ozone, similar to what was achieved for regional surface temperatures in Stone et al. (2019).

We construct a conditional empirical model for all years and calculate a HSS through a leave-three-out cross validation method for the ozone extreme years only. This is shown in Figure 7 for sea ice (a and b) and snow depth (c and d) in both observations and the model composite. A good proportion of predictions do not lie outside of the bootstrapped variability, highlighting that predictions of the cryosphere anomalies are not as robust as surface temperature predictions in Stone et al. (2019). However, good significant predictability is still achieved in areas expected from the largest differences shown in Figures 3 and 5, highlighted below.

For sea ice, we see that the most consistent predictions are occurring in the Bering Sea and the Sea of Okhotsk in June in observations and before June in the model, with HSSs of up to 35 in the model and 40 in the observations or around 67.5% and 70% correct predictions respectively. As the sea ice retreats into the Arctic ocean, the HSSs remain elevated until October in the model. In the Observations, the HSSs also remain elevated in agreement with the model, however, not significantly.

In the Barents-Kara Sea the most significant HSSs are occurring in April in the observations and April and May in the model composite, at around 40 in observations and 25 in the model composite. The HSSs then go mostly to 0, indicating that the predictability for this region is limited to only 1 or 2 months after the March TCO predictor.

For the Greenland Sea, the HSSs are effectively zero in both April and May in the observations and in April–June in the model composite. However, in the observations, the HSSs reach 70%, or 85% correct predictions in June and remain elevated through to September. In the model, the HSS peak in August at 20 and remain elevated through to October, however with little significance after July. The lower model ensemble predictive skill in the Greenland and Barents-Kara Seas compared to OBCLED can be attributed to the larger variability among ensemble members for these regions as shown in Figure 3.

Snow depth predictions are calculated for the sum of the same regions as shown in Figure 4. In the Northern Russian region, we see skill scores of up to 60 in the observations in April, whereas the model shows significant scores of up to 20 in April. In Southern Russia, significant skill scores are seen in April of 45 in the observations, and in April and May of up to 35 in the model ensemble. In South-East Alaska, observed skill scores of up to 55 are seen in June and July, or 77.5% correct predictions. In the model, significant skill scores of up to 20 are seen in April and May.

Similar to what was seen in Stone et al. (2019) for surface temperature, March TCO is able to predict the sign of sea ice extent and snow depth anomalies for some regions. The main differences between the cryosphere and surface temperatures are that the cryosphere overall shows a great deal more persistence, especially in sea ice extent, with differences being retained throughout the entire year and predictability being retained until fall in some locations.

5. Conclusions

Sea ice in the Arctic is currently undergoing large changes due to climate change (Kirtman et al., 2013). Therefore, understanding factors influencing the seasonal prediction of Arctic sea ice and other elements of the cryosphere are particularly important. Following the surface temperature anomaly predictions using March Arctic ozone in Stone et al. (2019), here we extend this work into the Arctic cryosphere using a 9-member ensemble of simulations from a state-of-the-art chemistry climate model (WACCM), and observations.

Previous work has shown large connections between the Arctic wintertime stratospheric polar vortex anomalies and future sea ice (Smith et al., 2018). Here, we use March TCO as a proxy for the wintertime polar vortex. TCO not only acts as a proxy for the polar vortex anomalies, but also for the state of the vortex over the entire winter, as shown in Figure 1. Since TCO is measured very frequently, accurately (and has been for decades), and in near real time, it is a prime candidate for investigating the influence of the wintertime stratosphere on the Arctic surface.

Seasonal differences in sea ice fraction during ozone extreme years (upper 20th percentiles minus the lower 20th percentiles) show excellent agreement between the model composite and the observations, as well as with Smith et al. (2018). The largest and most significant positive differences are found in the Bering Sea and the Sea of Okhotsk during April and May. As the sea ice retreats during summer, these differences are seen throughout the Laptev, East Siberian, Chukchi, and Beaufort Seas, and remain elevated through to November. The largest negative differences occur in the Greenland Sea with a maximum difference seen in July in observations, and in August and September in the model composite. The persistence of these features suggests that they could serve as a useful test bed to evaluate Arctic stratosphere-troposphere coupling behavior in different climate models.

Snow depth differences are also seen, with excellent agreement between the model and the observations in key locations, including negative differences seen in Northern Russia, and positive differences in Southern Russia and South East Alaska. The snow depth differences remain elevated until early summer, when snow cover diminishes.

The large differences in the cryosphere in the months following March ozone extremes, are also reflected in predictions of sea ice extent and snow depth anomalies. Using a simple regression model and March Arctic

ozone as the sole predictor, sea ice extent and snow depth is able to be predicted for observations and individual ensemble members in regions that show large correlations. This is especially notable for observations during 2011, which experienced large Arctic ozone depletion. However, there is large variability among ensemble members, indicating a more appropriate approach is to predict the sign of the sea ice fraction and snow depth anomalies.

The sign of the anomaly predictions are achieved through a leave-three-out cross validation method of an empirical prediction model using total column ozone as the sole predictor. Using this method, Heidke skill scores of up to 40 (70% correct predictions) in the observations and 35 (67.5% correct predictions) in the model composite are seen in the Bering Sea and corresponding seas further North and remain elevated in the model through to October, which could have implications for shipping routes. Significant predictions are also seen in the Greenland Sea during the early summer period, with observed 85% correct predictions, remaining elevated until September. In the Barents-Kara Sea, good prediction is only seen during April and May. For snow depth, we see the best predictions of the sign of the snow depth anomaly in Northern and Southern Russia during April and May, which is a similar location to where predictability was found in surface temperature in Stone et al. (2019). For South East Alaska, good predictability is seen during June and July in observations and during April and May in the model.

In summary, the results presented here show that springtime Arctic ozone can act as a good predictor for the regional cryosphere in parts of the Northern Hemisphere, with predictions in sea ice extent in particular being attainable throughout the year in some locations.

Data Availability Statement

MERRA2 data can be freely obtained online (at https://gmao.gsfc.nasa.gov/reanalysis/MERRA-2/data_access/). Model results shown in this paper are available online (at: http://doi.org/10.7910/DVN/V5R9WV).

Acknowledgments

K. S. and S. S. were partly supported by National Science Foundation grants 1419667, 1338814, and 1848863. D. K. was supported by National Science Foundation grant 1338814. WACCM is a component of the Cossmmunity Earth System Model (CESM), which is supported by the National Science Foundation. We would like to acknowledge high-performance computing support from Cheyenne (doi:http://10.5065/D6RX99HX) provided by NCAR's Computational and Information Systems Laboratory, sponsored by the National Science Foundation. We would like to thank Bodeker Scientific, funded by the New Zealand Deep South National Science Challenge, for providing the combined National Institute for Water and Atmosphere-Bodeker Scientific total column ozone database. The V3.2 patched data set can be obtained online (at http://www.bodekerscientific.com/data/total-column-ozone).

References

Baldwin, M. P., & Dunkerton, T. J. (2001). Stratospheric harbingers of anomalous weather regimes. *Science*, *294*(5542), 581–584. https://doi.org/10.1126/science.1063315

Bandoro, J., Solomon, S., Donohoe, A., Thompson, D. W. J., & Santer, B. D. (2014). Influences of the antarctic ozone hole on southern hemispheric summer climate change. *Journal of Climate*, *27*(16), 6245–6264. https://doi.org/10.1175/JCLI-D-13-00698.1

Broxton, P. D., Zeng, X., & Dawson, N. (2016). Why do global reanalyses and land data assimilation products underestimate snow water equivalent? *Journal of Hydrometeorology*, *17*(11), 2743–2761. https://doi.org/10.1175/jhm-d-16-0056.1

Calvo, N., Polvani, L., & Solomon, S. (2015). On the surface impact of Arctic stratospheric ozone extremes. *Environmental Research Letters*, *10*, 094003. https://doi.org/10.1088/1748-9326/10/9/094003

Charlton-Perez, A. J., Ferranti, L., & Lee, R. W. (2018). The influence of the stratospheric state on North Atlantic weather regimes. *Quarterly Journal of the Royal Meteorological Society*, *144*(713), 1140–1151. https://doi.org/10.1002/qj.3280

Cheung, J. C. H., Haigh, J. D., & Jackson, D. R. (2014). Impact of EOS MLS ozone data on medium-extended range ensemble weather forecasts. *Journal of Geophysical Research: Atmospheres*, *119*, 9253–9266. https://doi.org/10.1002/2014JD021823

Garcia, R. R., Smith, A. K., Kinnison, D. E., de la Cámara, Á., & Murphy, D. J. (2017). Modification of the gravity wave parameterization in the whole atmosphere community climate model: Motivation and results. *Journal of the Atmospheric Sciences*, *74*(1), 275–291. https://doi.org/10.1175/JAS-D-16-0104.1

Garfinkel, C. I., Waugh, D. W., & Gerber, E. P. (2013). The effect of tropospheric jet latitude on coupling between the stratospheric polar vortex and the troposphere. *Journal of Climate*, *26*(6), 2077–2095. https://doi.org/10.1175/JCLI-D-12-00301.1

Gelaro, R., McCarty, W., Suárez, M. J., Todling, R., Molod, A., Takacs, L., et al. (2017). The Modern-Era Retrospective Analysis for Research and Applications, version 2 (MERRA-2). *Journal of Climate*, *30*(13), 5419–5454. https://doi.org/10.1175/JCLI-D-16-0758.1

Gillett, Z. E., Arblaster, J. M., Dittus, A. J., Deushi, M., Jöckel, P., Kinnison, D. E., et al. (2019). Evaluating the relationship between interannual variations in the Antarctic ozone hole and Southern Hemisphere surface climate in Chemistry-Climate Models. *Journal of Climate*, *32*(11), 3131–3151. https://doi.org/10.1175/JCLI-D-18-0273.1

Haase, S., & Matthes, K. (2019). The importance of interactive chemistry for stratosphere-troposphere coupling. *Atmospheric Chemistry and Physics*, *19*(5), 3417–3432. https://doi.org/10.5194/acp-19-3417-2019

Harari, O., Garfinkel, C. I., Ziskin Ziv, S., Morgenstern, O., Zeng, G., Tilmes, S., et al. (2019). Influence of Arctic stratospheric ozone on surface climate in CCMI models. *Atmospheric Chemistry and Physics*, *19*(14), 9253–9268. https://doi.org/10.5194/acp-19-9253-2019

Hartley, D. E., Villarin, J. T., Black, R. X., & Davis, C. A. (1998). A new perspective on the dynamical link between the stratosphere and troposphere. *Nature*, *391*(6666), 471–474. https://doi.org/10.1038/35112

Ivy, D. J., Solomon, S., Calvo, N., & Thompson, D. W. J. (2017). Observed connections of Arctic stratospheric ozone extremes to Northern Hemisphere surface climate. *Environmental Research Letters*, *12*(2), 024,004. https://doi.org/10.1088/1748-9326/aa57a4

Jia, L., Yang, X., Vecchi, G., Gudgel, R., Delworth, T., Fueglistaler, S., et al. (2017). Seasonal prediction skill of northern extratropical surface temperature driven by the stratosphere. *Journal of Climate*, *30*(12), 4463–4475. https://doi.org/10.1175/JCLI-D-16-0475.1

Karpechko, A. Y., Perlwitz, J., & Manzini, E. (2014). A model study of tropospheric impacts of the Arctic ozone depletion 2011. *Journal of Geophysical Research: Atmospheres*, *119*, 7999–8014. https://doi.org/10.1002/2013JD021350

Kelleher, M. E., Ayarzaguena, B., & Screen, J. A. (2020). Interseasonal connections between the timing of the stratospheric final warming and Arctic Sea ice. *Journal of Climate*, *33*, 3079–3092. https://doi.org/10.1175/JCLI-D-19-0064.1

Kirtman, B., Power, S. B., Adedoyin, J. A., Boer, G. J., Bojariu, R., Camilloni, I., et al. (2013). Near-term climate change: Projections and predictability. In T. F. Stocker, D. Qin, G. K. Plattner, M. Tignor, S. K. Allen, J. Boschung, et al. (Eds.), *Climate change 2013: The physical science basis. Contribution of Working Group I to the Fifth Assessment Report of the Intergovernmental Panel on Climate Change* (pp. 953–1028). Cambridge, United Kingdom and New York, NY, USA: Cambridge University Press. https://doi.org/10.1017/CBO9781107415324.023

Kwok, R. (2000). Recent changes in Arctic Ocean sea Ice motion associated with the North Atlantic Oscillation. *Geophysical Research Letters*, *27*, 775–778.

Ma, X., Xie, F., Li, J., Zheng, X., Tian, W., Ding, R., et al. (2019). Effects of Arctic stratospheric ozone changes on spring precipitation in the northwestern United States. *Atmospheric Chemistry and Physics*, *19*(2), 861–875. https://doi.org/10.5194/acp-19-861-2019

Marsh, D. R., Mills, M. J., Kinnison, D. E., Lamarque, J.-F., Calvo, N., & Polvani, L. M. (2013). Climate change from 1850 to 2005 simulated in CESM1(WACCM). *Journal of Climate*, *26*, 7372–7391. https://doi.org/10.1175/JCLI-D-12-00558.1

Morgenstern, O., Hegglin, M., Rozanov, E., O'Connor, F., Luke Abraham, N., Akiyoshi, H., et al. (2017). Review of the global models used within phase 1 of the Chemistry-Climate Model Initiative (CCMI). *Geoscientific Model Development*, *10*(2), 639–671. https://doi.org/10.5194/gmd-10-639-2017

Perlwitz, J., & Harnik, N. (2003). Observational evidence of a stratospheric influence on the troposphere by planetary wave reflection. *Journal of Climatenal of Climate*, *13*(1998), 3011–3026. https://doi.org/10.1175/1520-0442(2003)016<3011:OEOASI>2.0.CO;2

Plumb, R. A., & Semeniuk, K. (2003). Downward migration of extratropical zonal wind anomalies. *Journal of Geophysical Research*, *108*(7), 4223. https://doi.org/10.1029/2002JD002773

Polvani, L. M., & Waugh, D. W. (2004). Upward wave activity flux as a precursor to extreme stratospheric events and subsequent anomalous surface weather regimes. *Journal of Climate*, *17*(18), 3548–3554. https://doi.org/10.1175/1520-0442(2004)017<3548:UWAFAA>2.0.CO;2

Rigor, I. G., Wallace, J. M., & Colony, R. L. (2002). Response of sea ice to the Arctic Oscillation. *Journal of Climate*, *15*(18), 2648–2663. https://doi.org/10.1175/1520-0442(2002)015<2648:ROSITT>2.0.CO;2

Romanowsky, E., Handorf, D., Jaiser, R., Wohltmann, I., Dorn, W., Ukita, J., et al. (2019). The role of stratospheric ozone for Arctic-midlatitude linkages. *Scientific Reports*, *9*(1), 7962. https://doi.org/10.1038/s41598-019-43823-1

Scaife, A. A., Karpechko, A. Y., Baldwin, M. P., Brookshaw, A., Butler, A. H., Eade, R., et al. (2016). Seasonal winter forecasts and the stratosphere. *Atmospheric Science Letters*, *17*(1), 51–56. https://doi.org/10.1002/asl.598

Sigmond, M., Scinocca, J. F., Kharin, V. V., & Shepherd, T. G. (2013). Enhanced seasonal forecast skill following stratospheric sudden warmings. *Nature Geoscience*, *6*, 98–102. https://doi.org/10.1038/ngeo1698

Smith, K. L., Polvani, L. M., & Tremblay, L. B. (2018). The impact of stratospheric circulation extremes on minimum arctic sea ice extent. *Journal of Climate*, *31*(18), 7169–7183. https://doi.org/10.1175/JCLI-D-17-0495.1

Stone, K. A., Solomon, S., Kinnison, D. E., Baggett, C. F., & Barnes, E. A. (2019). Prediction of Northern Hemisphere regional surface temperatures using stratospheric ozone information. *Journal of Geophysical Research: Atmospheres*, *124*, 5922–5933. https://doi.org/10.1029/2018JD029626

Stroeve, J. C., Maslanik, J., Serreze, M. C., Rigor, I., Meier, W., & Fowler, C. (2011). Sea ice response to an extreme negative phase of the Arctic Oscillation during winter 2009/2010. *Journal of Geophysical Research*, *38*, L02502. https://doi.org/10.1029/2010GL045662

Struthers, H., Bodeker, G. E., Austin, J., Bekki, S., Cionni, I., Dameris, M., et al. (2009). The simulation of the Antarctic ozone hole by chemistry-climate models. *Atmospheric Chemistry and Physics*, *9*(17), 6363–6376. https://doi.org/10.5194/acp-9-6363-2009

Thompson, D. W. J., Solomon, S., Kushner, P. J., England, M. H., Grise, K. M., & Karoly, D. J. (2011). Signatures of the Antarctic ozone hole in Southern Hemisphere surface climate change. *Nature Geoscience*, *4*(11), 741–749. https://doi.org/10.1038/ngeo1296

Wettstein, J. J., & Deser, C. (2014). Internal variability in projections of twenty-first-century Arctic Sea ice loss: Role of the large-scale atmospheric. *Circulation*, *27*, 527–550. https://doi.org/10.1175/JCLI-D-12-00839.1

Williams, J., Bruno, T., Newton, R., & Richard, A. (2016). Dynamic preconditioning of the minimum September sea-ice extent. *Journal of Climate*, *29*, 5879–5891. https://doi.org/10.1175/JCLI-D-15-0515.1

Xie, F., Zhang, J., Sang, W., Li, Y., Qi, Y., Sun, C., et al. (2017). Delayed effect of Arctic stratospheric ozone on tropical rainfall. *Atmospheric Science Letters*, *18*(10), 409–416. https://doi.org/10.1002/asl.783

Zhang, P., Wu, Y., Simpson, I. R., Smith, K. L., Zhang, X., De, B., & Callaghan, P. (2018). A stratospheric pathway linking a colder Siberia to Barents-Kara Sea sea ice loss. *Science Advances*, *4*(7), 1–9. https://doi.org/10.1126/sciadv.aat6025